

See discussions, stats, and author profiles for this publication at: <https://www.researchgate.net/publication/373521032>

Remote sensing-based geostatistical hot spot analysis of Urban Heat Islands in Dhaka, Bangladesh

Article in *Singapore Journal of Tropical Geography* · August 2023

DOI: 10.1111/sjtg.12507

CITATIONS

8

READS

343

3 authors:



Nur Hussain
McMaster University

1 PUBLICATION 8 CITATIONS

[SEE PROFILE](#)



S.M. Shahriar Ahmed
Center for Environmental and Geographic Information Services

3 PUBLICATIONS 16 CITATIONS

[SEE PROFILE](#)



Amena Muzaffar Shumi
1 PUBLICATION 8 CITATIONS

[SEE PROFILE](#)



Remote sensing-based geostatistical hot spot analysis of Urban Heat Islands in Dhaka, Bangladesh

Nur Hussain,¹ S.M. Shahriar Ahmed² and Amena Muzaffar Shumi^{3†}

¹School of Earth, Environment & Society, McMaster University, Hamilton, Canada

²Department of Geography and Environment, Jahangirnagar University, Dhaka, Bangladesh

³Faculty of Agricultural Sciences, University of Hohenheim, Stuttgart, Germany

Correspondence: Nur Hussain (email: nurhussain55@gmail.com)

Urban Heat Island (UHI) refers to a phenomenon whereby urban areas experience higher temperatures compared to the surrounding areas. Remote sensing-based Land Surface Temperature (LST) measurements can be utilized to measure UHI. This study emphasized on geostatistical remote sensing-based hot spot analysis (G_i^*) of UHI in Dhaka, Bangladesh as a way of examining the influences of Land Use Land Cover (LULC) on UHI from 1991 to 2015. Landsat 5 and 7 satellite-based remote sensing indices were used to explore LULC, UHI and environmental footprints during the study period. The Urban Compactness Ratio (C_{oR}) was used to calculate the urban form and augmented characteristics. The Surface Urban Heat Island (SUHI) intensity (ΔT) was also used to explore the effects of UHI on the surrounding marginal area. Based on our investigations into LULC, we discovered that around 71.34 per cent of water bodies and 71.82 percent of vegetation cover decreased from 1991 to 2015 in Dhaka city. Contrastingly, according to C_{oR} readings, 174.13 km² of urban areas expanded by 249.77 per cent. Our hot spot analysis also revealed that there was a 93.73 per cent increase in hot concentration zones. Furthermore, the average temperature of the study area had increased by 3.26°C. We hope that the methods and results of this study can contribute to further research on urban climate.

Keywords: urban expansion, urban heat island, hot spot analysis, ecological imbalance, urban metabolism

Accepted: 9 February 2023

Introduction

A key aspect of urbanization involves people migrating from rural to urban regions and cities (Elmqvist *et al.*, 2013; Vinayak *et al.*, 2022). In recent decades, urbanization has risen dramatically. Currently, over 56 percent of the world's population resides in urban areas, and this percentage is projected to rise to 68 percent by 2050 (UN-Habitat, 2020). Urbanization is associated with extensive land use land cover (LULC) changes (Deng & Srinivasan, 2016). Remote sensing-based indices help to measure changes in LULC and environmental footprints. The Normalized Difference Vegetation Index (NDVI) has become the most widely used index in vegetation, forestry, and agricultural research (Gao, 1996; Carlson & Arthur, 2000). Notably, the Normalized Difference Water Index (NDWI), Normalized Difference Built-up Index (NDBI), and Normalized Difference Bareness Index (NDBaI) were developed based on the NDVI model. The NDVI, NDWI, NDBI, and NDBaI describe the physical footprints or

[†]Current affiliation: Data Science, Don Valley Advanced Solutions (DVAS), Toronto, Canada.

critical indicators of land cover distribution and changes in LULC (Cao *et al.*, 2002; Deng & Wu, 2012; Zhao & Chen, 2005). LULC measurements indicate changes in the urban physical landscape and growth rate of urban built-up areas compared to other physical footprints. Urban compactness is one of the leading indicators of urban growth rate (Chen, 2011; Du *et al.*, 2016). The consequence of urban compactness expansion is explained in urban metabolism (Wolman, 1965). Urban LULC influences the urban area's Land Surface Temperature (LST) (Shahfahad *et al.*, 2022a).

The urban LST depends on changes in urban LULC, environmental circumstances and ecological conditions (Qian *et al.*, 2006). The relationship between LST and LULC ratifies NDVI, NDWI, NDBI, and NDBal indices (Gillies & Carlson, 1995; Chen *et al.*, 2006a). Unplanned LULC and/or haphazard urbanization is a leading cause in the formation of LST-based heat islands in many city areas. Urban Heat Islands (UHIs) are the most prominent example of local weather changes associated with urbanization, in which urban areas experience greater temperatures than the surrounding rural regions (Howard, 1833; Meng *et al.*, 2018). According to Souch and Grimmond (2006), the UHI can occur at any time of year, depending on local weather conditions. Generally, higher temperatures in the urban core commercial areas and lower temperatures in rural areas are considered as UHIs (Souch & Grimmond, 2006). UHIs occur when built structures cause the destruction of green cover and wetlands inside the urban area and its surrounding periphery (Jones *et al.*, 1990). The urban structural land surface absorbs maximum heat in the daytime and increases low atmospheric air temperature at night by surface absorbed heat release (Sobstyl *et al.*, 2018), which can affect local weather and climate (Liu & Zhang, 2011; Rosenzweig *et al.*, 2008; Rayk *et al.*, 2016; Streutker, 2002). Luke Howard (1833) first proposed the concept of UHI in 1833. However for many years there was less work on UHIs in tropical cities than in temperate zones. UHI research was conducted in 1964 by Nieuwolt (1966) in Singapore's southern urban area (Chen *et al.*, 2006b; Roth *et al.*, 2012). In the early 1980s, climatologists used the UHI study's energy and water balance processes to calculate urban heat storage (Oke & Cleugh, 1987). When an UHI exists within a city, the temperature difference is generally more significant at night in the winter and when the winds are weaker at night than daytime in summer (Streutker, 2002). However, different scenarios can exist depending on the spatio-temporal context of analysis.

Thermal remote sensing-based UHI was developed in the early 1990s and has continuously improved. Several studies have employed remote sensing-based UHI in their investigations on various cities, i.e. Singapore (Goh & Chang, 1999; Shahfahad *et al.*, 2022b), Texas (Streutker, 2002), Hong Kong (Nichol & Wong, 2005), Guangzhou, Boluo, Dongguan, Panyu, Foshan, Gaoming, Huadu, Huizhou, Nanhai and Sanshui in Guangdong Province (Zhang & Wang, 2008), Dhaka-Bangladesh (Ahmed *et al.*, 2013), the Salt Lake basin area of Turkey (Orhan *et al.*, 2014), Budapest, Ljubljana, Modena, Padua, Prague, Stuttgart, Vienna, and Warsaw (Damyanovic *et al.*, 2016; Mahdavi *et al.*, 2016), North-western Siberian cities (Miles & Esau, 2017), Beijing (Meng *et al.*, 2018), and Shanghai (Tan *et al.*, 2010). These studies were conducted using satellite-retrieved LST concentration. LST-based UHI has also recently been applied in multi-disciplinary research areas: i.e. urban expansion and UHI intensity (Li *et al.*, 2018; Hu & Brunsell, 2015), phenology of urban ecosystems, spatial and temporal pattern distribution of UHI (Santos *et al.*, 2017; Yao *et al.*, 2017), urban atmospheric profile (Hu & Brunsell, 2015), urban weather and climatic zone (Chen *et al.*, 2014; Bechtel *et al.*, 2015; Huang *et al.*, 2017), vegetative cover (Maimaitiyiming *et al.*, 2014; Lu *et al.*, 2017) and urban land use/urban metabolism (Fu & Weng, 2017);

Tran *et al.*, 2017). Ord and Getis (1995) proposed a model of local spatial autocorrelation statistics. Urban metabolism emphasizes city transformation, city expansion, and environmental degradation within input-throughput-output appearance (Newman, 1999; Decker *et al.*, 2000). The UHI distribution is responsible for urban ecological degradation, local climate change, micro-level biodiversity, and ecological imbalance. The physical features of LULC are one of the central derivations of urban ecological footprints (Wackernagel *et al.*, 2002; Holden, 2004; Chen *et al.*, 2006b) associated with urban metabolism and urban sustainability. Hence, UHI assessment is imperative for ecological conservation and sustainability in urban expansion.

A hot spot can be defined as an area with a higher temperature concentration than the average temperature zone calculated from a random distribution of the study site (Hussain & Islam, 2020; Chakravorty, 1995). The hot spot method is an autocorrelation analysis conducted to explore the interactions and relations among the distribution of variability in a geospatial location (Baddeley, 2010). Geographic Information System (GIS) applications have dramatically expanded the use of hot spots (G_i^*) in recent decades, especially for geostatistical analysis. The hot spot (G_i^*) analysis comes from geostatistical and geospatial autocorrelation models. This local spatial autocorrelation model stands on G_i^* (d) and G (d) statistics as first introduced by Getis and Ord (1992). In 2005, Arc User (ESRI) extended spatial analysis tools in ArcGIS spatial statistical analysis segments (Scott & Warmerdam, 2005) according to the local spatial autocorrelation G_i^* (d) and G (d) statistics. These spatial analysis tools include hot spot (G_i^*) analysis allowing the spatial autocorrelation method to delineate spatial clusters of nearest neighbouring objects (Hussain & Islam, 2020). In this study, geostatistical hot spot analysis was used to detect UHI effects over 25 years, helping policymakers to conduct better prediction and urban planning strategies.

In this study, we analyse the trends of UHI in Dhaka city using hot spot (G_i^*) analysis. Dhaka is rapidly growing and one of the most densely populated megacities globally (Taleb, 2012; Hossain, 2008; Ahmed *et al.*, 2013). To the authors' knowledge, there appears to be only one UHI-related research work relating to the Dhaka megacity, conducted by Ahmed *et al.* (2013). Ahmed *et al.* (2013) provided UHI and land-use status change based on yearly one-day remote sensing data for 10-year intervals from 1989 to 2009. In this research, we calculated UHI effects based on 25 years of data (1991 to 2015) with seasonal variation of the spatial and temporal distribution of heat islands and compared UHI and temperature variations within the rural-urban fringe area. The Surface Urban Heat Island (SUHI) intensity (ΔT) indicates the effect of UHI on the concentration of the surrounding marginal area (Peng *et al.*, 2012). Our research focuses on urban expansion, land-use change, UHI distribution, and SUHI intensity. These circumstances are significant for environmental conservation and socio-ecological sustainability. Accordingly, the main objectives of this study are to: 1) explore changes in LULC, urban expansion and compactness from 1991–2015 based on remote sensing data; 2) explore the relationship between land cover changes and variations in LST; 3) determine UHI distribution using hot spot (G_i^*) and 4) calculate seasonal SUHI intensity (ΔT) during the last 25 years from 1991–2015.

Data and methodology

Study area

This study focuses on the anthropogenetic and environmental context of the Dhaka megacity. Dhaka, the capital city of Bangladesh, is one of the most densely populated

and rapidly growing megacities in the world (Ahmed *et al.*, 2013). According to the Bangladesh Bureau of Statistics, Dhaka megacity's total population in 1991, 2001, and 2011 was 6 620 697, 10 284 947 and 14 730 537 respectively. It reached 17 million in 2017, and has continued to grow since. The study area is located in the tropical humid climatic zone between $23^{\circ} 40'$ north and $23^{\circ} 54'$ north latitude and $90^{\circ} 20'$ east and $90^{\circ} 30'$ east longitude (Figure 1), bounded by the *Buriganga* River, *Turag* River, *Dhaleshwari River*, and *Shitalakshya* River (Hussain, 2018). During the study period (1991–2015), the average temperatures recorded in the winter, summer, and autumn

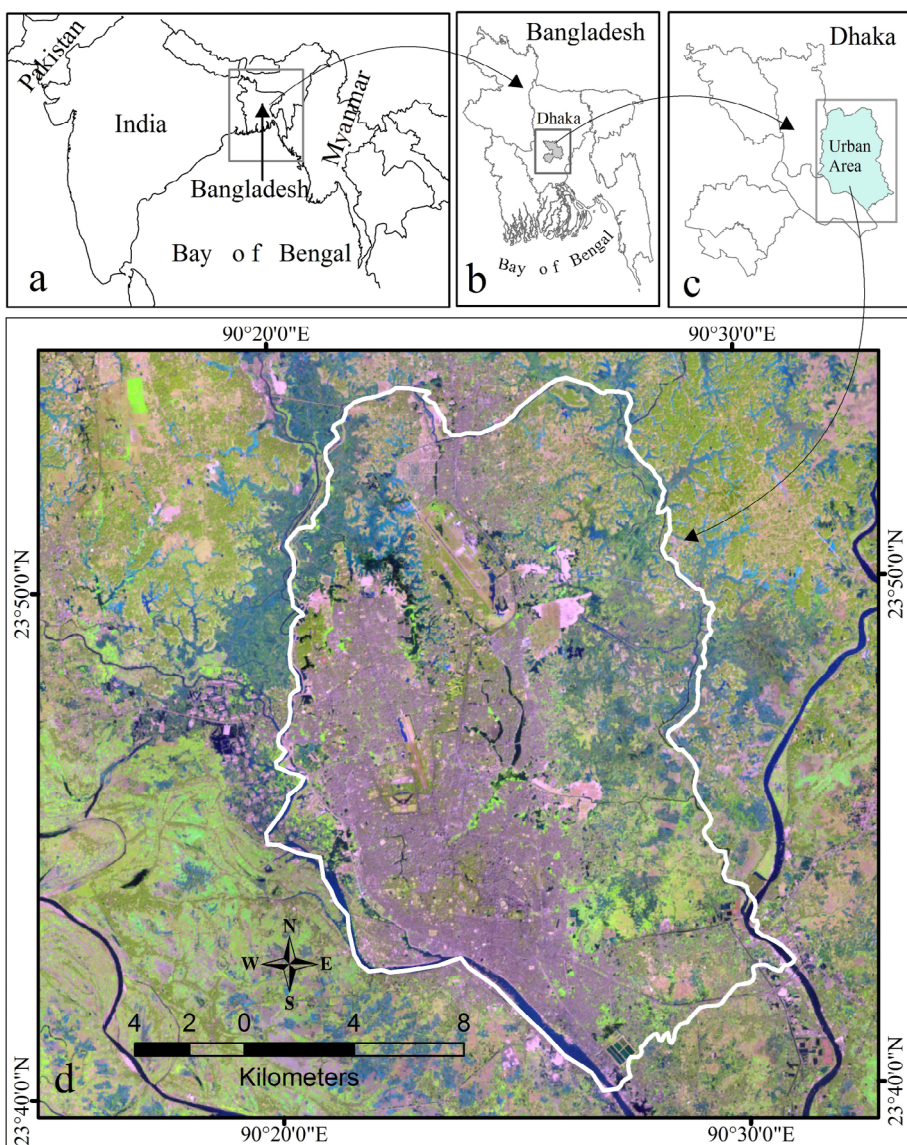


Figure 1. Map depicting a) Bangladesh, b) Dhaka c) Dhaka's urban area, and d) Landsat-5, 30m spatial resolution image with RGB 543 band spectrum of Dhaka's urban area.

seasons were 23.8°C, 28.7°C and 24.2°C respectively. According to Shuttle Radar Topography Mission (SRTM) data, the mean elevation of the study area is 11 meters above the mean sea level (Figure 4b).

Data

In this study, we investigated urban expansion, urban compactness ratio (C_{oR}), land surface temperature (LST) and land use land cover (LULC) change using Landsat 5 and Landsat 7 data. Urban physical footprints were detected using the same remote sensing data with suppositional vital indicators of physical footprints, such as NDVI, NDWI, NDBI, and NDBaI to explore the relationship between UHI characteristics and these indices. While the Digital Elevation Model (DEM) of the study area was extracted using the SRTM data, SUHI intensity (ΔT) was calculated using the retrieved LST. Hot spot analysis (G_i^*) was also explored using LST within the geostatistical analysis of Arc GIS 10.4 (Esri). Table 1 represents Landsat 5, Landsat 7, and SRTM data references with acquisition dates. Landsat 5 satellite images were used for the years 1991, 1995, 1999, 2007, and 2011 while Landsat 7 satellite images were used for the years 2003 and 2015 as Landsat 5 data were not available for 2003 and 2015 (USGS, 2011). All data types were analysed at four-year intervals to understand the urban phenomenon's short and long temporal changing characteristics (Table 1). Unprocessed raw data were download from the United States Geological Survey (USGS) website; URL (<https://earthexplorer.usgs.gov/>).

Data analysis

The research process is summarized in Figure 2. Satellite data were acquired from Landsat 5, Landsat 7, and SRTM in four-year intervals from 1991 to 2015. For each year, three sets

Table 1. Data reference.

Data Type	Spatial resolution	Path/Row	Acquisition Date
Landsat 5	30m	137/044	Jan 26, 1991
	60m for thermal band	137/044	Apr 16, 1991
		137/044	Aug 22, 1991
		137/044	Jan 05, 1995
		137/044	Apr 11, 1995
		137/044	Sep 02, 1995
		137/044	Feb 01, 1999
		137/044	Apr 22, 1999
		137/044	Oct 15, 1999
		137/044	Jan 22, 2007
		137/044	Apr 28, 2007
		137/044	Sep 19, 2007
Landsat 7	30m	137/044	Jan 17, 2011
	60m for thermal band	137/044	May 09, 2011
		137/044	Sep 30, 2011
		137/044	Jan 19, 2003
		137/044	May 11, 2003
		137/044	Aug 15, 2003
SRTM	~30m		
		137/044	Feb 05, 2015
		137/044	May 28, 2015
		137/044	Sep 17, 2015
			Sep 23, 2014

Source: Table produced by author based on U.S. Geological Survey [<https://earthexplorer.usgs.gov/>].

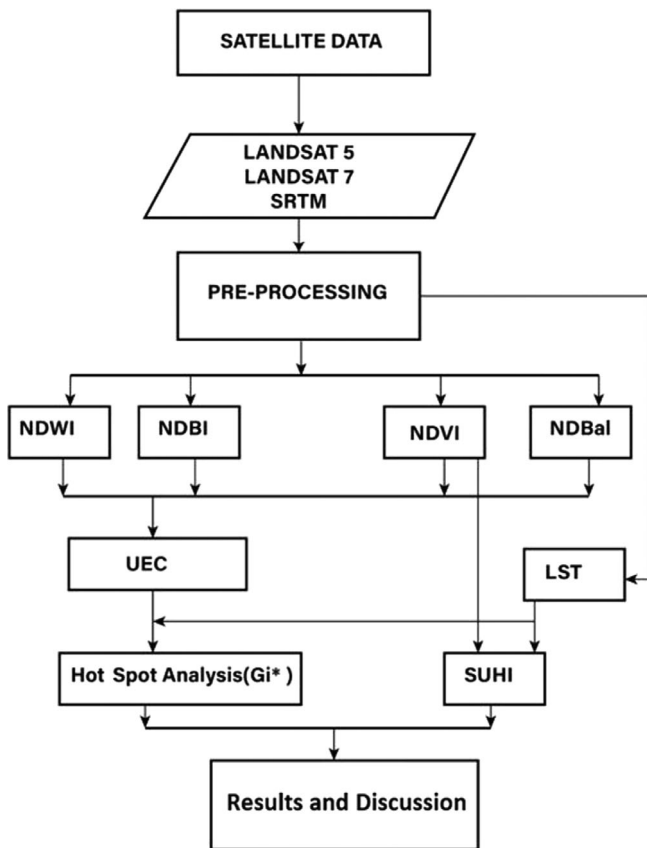


Figure 2. Research methods.

of data were obtained for summer, autumn, and winter. The satellite data went through pre-processing steps consisting of atmospheric and radiometric corrections. NDVI, NDWI, NDBI, and NDBal were extracted using processed datasets. LST was also retrieved from processed thermal bands of Landsat images. LST-based temperature anomalies were used for hot spot (G_i^*) analysis to find the significant and non-significant areas. LST and NDVI indices were used for exploring Surface Urban Heat Island (SUHI).

Land use land cover (LULC) change. Land cover change was extracted using Landsat 5 and Landsat 7 data. Both datasets were analysed in ArcMap 10.7 (Esri) and land cover was detected using supervised classification. NDVI, NDWI, NDBI, and NDBal were calculated using the same series of data. NDVI was calculated using visible red bands (0.63 μm - 0.69 μm) and near-infrared bands (0.76 μm - 0.90 μm) of Landsat 5 and 7 data according to Equation 1 (Kogan, 1995). NDWI was calculated using near-infrared band (0.76 μm - 0.90 μm) and short-wave infrared band-1 (1.55 μm - 1.75 μm) conforming to Equation 2 (McFeeters, 1996). NDBI was calculated using near-infrared band (0.76 μm - 0.90 μm) and short-wave infrared band-1 (1.55 μm - 1.75 μm) following Equation 3 (Zha *et al.*, 2003). NDBal was calculated using short wave infrared band-1 (1.55 μm - 1.75 μm) and thermal band (10.40 μm - 12.50 μm) calibrating to Equation 4 (Zhao & Chen, 2005).

$$NDVI = \frac{b_4 - b_3}{b_4 + b_3} \quad (1)$$

$$NDWI = \frac{b_4 - b_5}{b_4 + b_5} \quad (2)$$

$$NDBI = \frac{b_5 - b_4}{b_5 + b_4} \quad (3)$$

$$NDBaI = \frac{b_5 - b_6}{b_5 + b_6} \quad (4)$$

where b_3 are visible red bands ($0.63 \mu\text{m}$ - $0.69 \mu\text{m}$), b_4 is the near-infrared band ($0.76 \mu\text{m}$ - $0.90 \mu\text{m}$), b_5 is the short wave infrared band-1 ($1.55 \mu\text{m}$ - $1.75 \mu\text{m}$) and b_6 is the thermal band ($10.40 \mu\text{m}$ - $12.50 \mu\text{m}$).

Urban expansion and compactness. The compactness ratio is a proportion used to measure the spatial form and density of urban areas calculated by dividing the total area and built-up area. In this study, we analysed compactness (i) to determine the direction of urban expansion and extension of built-up areas during the 4-year interval and also (ii) to explore the actual changes in the urban centre. The urban expansion ratio was analysed using Landsat 5 and Landsat 7 data. The elevation of the expansion area was detected using DEM. The DEM works in tandem with the Triangular Irregular Networks (TIN) method. This formula of compactness ratio (C_{oR}) put forward by Richardson in 1961 (see Haggett *et al.*, 1977) was applied to calculate urban form and augmented characteristics (Chen, 2011). The urban compactness ratio (C_{oR}) can be calculated using the following equation:

$$C_{oR} = \frac{2\sqrt{\pi A}}{P} \quad (5)$$

where C_{oR} is the compactness ratio, A is Area and P is the perimeter of the urban area.

Retrieval of LST. Chen *et al.* (2002) proposed a method to simulate brightness temperature for the retrieval of LST using Landsat 5 data. Firstly, the digital number (DN) of the thermal band ($10.40 \mu\text{m}$ - $12.50 \mu\text{m}$) is used to convert radiation to luminance using the following formula:

$$R_{TM6} = \frac{V}{255} (R_{max} - R_{min}) \quad (6)$$

where V represents the DN of the thermal band, $R_{max} = 1.896 (\text{mW} \times \text{cm}^{-2} \times \text{sr}^{-1})$ and $R_{min} = 0.1534 (\text{mW} \times \text{cm}^{-2} \times \text{sr}^{-1})$. Then, the radiation luminance is converted to brightness temperature in Kelvin, T (K), using the following equation:

$$T = \frac{k1}{In \left(\frac{k2}{R_{TM6}} + 1 \right)} \quad (7)$$

Where T is the effective at-satellite temperature in Kelvin, $k1 = 1260.56$ (Calibration constant 2) and $k2 = 607.66$ (Calibration constant 1), both of which are

pre-launch calibration constants under an assumption of unity emissivity. Lastly, Kelvin is converted to Degree Celsius using the following equation:

$$T_c = T - 273.15 \quad (8)$$

where T is the effective at-satellite temperature in Kelvin and T_c is the temperature in degree Celsius.

The National Aeronautics and Space Administration (NASA) and the United States Geological Survey (USGS) proposed retrieving LST from Landsat 7 data. This method converts simulated image pixels into absolute radiance units using 32-bit floating-point calculations (USGS, 2011). Subsequently, pixel values of the simulated image are scaled by their values before media output using the following equations:

$$L_\lambda = Grescale \times QCAL + Brescale \quad (9)$$

$$L_\lambda = \frac{LMAX - LMIN}{QCALMAX - QCALMIN} \times (QCAL - QCALMIN) + LMIN \quad (10)$$

where L_λ is the Spectral Radiance at the sensor's aperture in watts/ (meter squared * ster * μm); *Grescale* and *Brescale* can be obtained from the header file of the satellite image; $QCALMIN = 1$ (minimum quantized calibrated pixel value); $QCALMAX = 255$ (maximum quantized calibrated pixel value); $QCAL$ = the quantized calibrated pixel value or DN, $LMAX$ = the spectral radiance that is scaled to $QCALMAX$ in watts/(meter squared * ster * μm); and $LMIN$ = the spectral radiance that is scaled to $QCALMIN$ in watts/(meter squared * ster * μm). $QCALMIN$, $QCALMAX$, $QCAL$, $LMAX$, and $LMIN$ values are also given in the images' header file.

Subsequently, the spectral radiance of the sensor was converted to brightness temperature in Kelvin, T (K), using the following equation:

$$T = \frac{k2}{In\left(\frac{k1}{L_\lambda} + 1\right)} \quad (11)$$

where T = effective at-satellite temperature in Kelvin; $K1 = 1260.56$ (Calibration constant 2); and $K2 = 607.66$ (Calibration constant 1), both of which are pre-launch calibration constants under an assumption of unity emissivity. Lastly, Kelvin is converted to Degree Celsius using Equation 8.

Hot spot (G_i^) analysis.* In 2005 ESRI Arc user developed the hot spot analysis (G_i^*) model to explore geospatial patterns (Scott & Warmerdam, 2005). The hot spot analysis (G_i^*) calculates high or low values of the cluster within the context of neighbouring data. The algorithm calculates geostatistical hot spots using the nearest neighbours autocorrelation model. The temperature concentration zone was investigated using hot spot (G_i^*) analysis following equations:

$$G_i^* = \frac{\sum_{j=1}^n w_{ij}x_j - \bar{X} \sum_{j=1}^n w_{ij}}{S \sqrt{\left[n \sum_{j=1}^n w_{ij}^2 - \left(\sum_{j=1}^n w_{ij} \right)^2 \right] / (n-1)}} \quad (12)$$

$$\bar{X} = \frac{\sum_{j=1}^n x_j}{n} \quad (13)$$

$$S = \sqrt{\sqrt{\frac{\sum_{j=1}^n x_j^2}{n}} - (\bar{X})^2} \quad (14)$$

where G_i^* are the hot spots and cold spots of spatial autocorrelation statistics; x_j is the attribute value for feature j ; $w_{i,j}$ is the spatial weight between feature i and j ; and n = total features.

SUHI intensity (ΔT) calculation. SUHI intensity (ΔT) is calculated as the difference in mean temperature between the Urban Main Built-up Area (UMBA) and the suburban boundary area (Meng *et al.*, 2018). Peng *et al.* (2012) found that the minimum influence area of the SUHI effect is 150 percent of the urban area (Peng *et al.*, 2012). Following this concentration, SUHI was measured with a 150 per cent buffer area surrounding Dhaka metropolitan city. Therefore, SUHI intensity (ΔT) was calculated using the following equation:

$$\Delta T = T_{Urban} - T_{Boundary} \quad (15)$$

where ΔT is SUHI intensity, T_{Urban} is the mean LST of the UMBA and $T_{Boundary}$ is the LST of the urban influencing neighbouring area.

Accuracy assessment of change detection

Generally, classification approaches of change detection have focused on the per-pixel process. The change vector analysis is advantageous for data visualization and attributes calculation of changes (Kontoes, 2008). However, the difference vector analysis technique provides a prolific window for geostatistical analysis. This study used change vector analysis to retrieve change detection from classified data sets. The traditional methods of accuracy assessment involve storing, analysing, and presenting spatial data of maps. The validation of land cover classification is required to establish the results. Validation is realized by comparing the classified image against the reference ground truth data. In the present study, we selected a total of 410 ground truth points, whereby 100 points were delineated for each land classification. The confusion matrix (*classification accuracy* = *correct prediction* / *total prediction*) was used to calculate precision, the user's and producer's classification accuracy, and overall classification accuracy (Table 2).

Results

Changes in land cover and physical footprints

Figure 3 and Table 4 represent the land cover changes of the Dhaka Metropolitan (DMP) area within seven different periods from 1991 to 2015 in four-year intervals. Land cover has been classified into four physical features: water bodies, vegetation, built-up areas, and bare soil. It can be observed from the results that the land cover of the DMP area changed rapidly. In 1991, seasonal and permanent water bodies covered 82.78 km² of the area; however, this area decreased to 23.94 km² in 2015.

Table 2. Average classification accuracy (1991–2015).

Year	User's Accuracy (%)				Producer's Accuracy (%)				Overall Accuracy (%)
	Water Body	Vegetation	Built-up Area	Bare Soil	Water Body	Vegetation	Built-up Area	Bare Soil	
1991	86.5	77.9	81.5	90.5	94.5	90	91.5	85.6	89.4
1995	86.1	86.2	82.9	91.1	90.5	96.5	90.6	91.2	91.4
1999	83.5	84.3	86.5	90.2	91	82.5	92.4	86.5	89.5
2003	90.2	88.7	89.2	87.5	88.5	79.2	88.6	91.2	86.5
2007	88.2	86.5	93.5	88.6	89.1	77.5	89.5	88.6	90.1
2011	86.5	83.4	91.6	90.5	90.2	81.7	90.2	87.1	88.3
2015	88.95	83.8	85.93	93	91.6	96.3	93.2	91.5	93.1

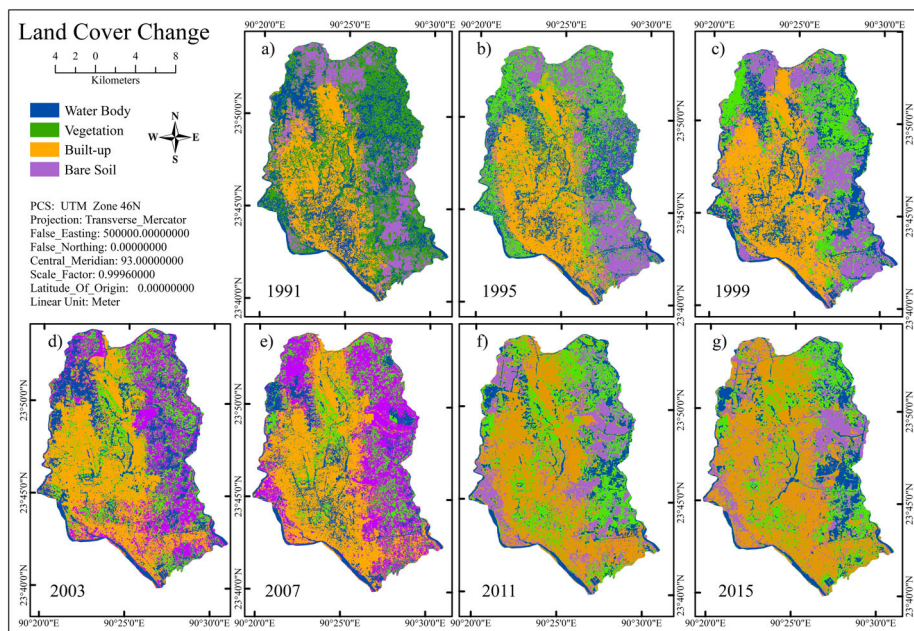


Figure 3. Land cover changes (1991–2015).

Vegetation coverage reduced from 101.91 km² to 28.72 km² in the last 25 years. Contrastingly, there was an increase in urban built-up and bare soil areas. From 1991 to 2015, urban built areas increased from 69.32 km² to 171.50 km², while bare soil areas increased from 48.25 km² to 77.84 km² (Figure 3 and Table 3).

Ahmed *et al.* (2013) found similar land cover changes in their study of Dhaka city using a 10-year interval from 1989 to 2009. In order to showcase more specific changing trends in land cover, we conducted our study across a four-year interval time series. According to field observations in 2016, most of the wetlands-dominated lowlands in Dhaka urban area had been converted to bare soil by unauthorized landfilling, during last three decades. Eventually most of these were transformed into built-up areas. Despite the issuance of stop orders by the High Court, illegal landfilling activities

Table 3. Land cover change in km² (1991–2015).

Year	Water Body		Vegetation		Built-up Area		Bare Soil	
	Area	Percentage	Area	Percentage	Area	Percentage	Area	Percentage
1991	82.78	27.41	101.91	33.74	69.32	22.95	48.25	15.98
1995	65.32	21.63	80.35	26.61	89.17	29.53	67.37	22.31
1999	63.37	20.98	64.48	21.35	103.92	34.41	70.45	23.33
2003	57.56	19.06	53.86	17.83	113.12	37.46	77.68	25.72
2007	41.39	13.71	45.79	15.16	122.94	40.71	92.10	30.50
2011	34.88	11.55	39.66	13.13	128.83	42.66	98.84	32.73
2015	23.94	7.93	28.72	9.51	171.50	56.79	77.84	25.77

have continued transforming the city's ecological and urban structure (Karim, 2003; UNESCAP 2003; *The Daily Star*, 2012, 2019; GoB, 2010). To make matters worse, developers are particularly interested in wetlands and areas with vegetation project areas as land prices there tend to be lower as compared to prices of areas in more elevated land.

Urban expansion and compactness

Urban expansion was traced using geospatial analysis. Urban compactness areas expanded from 116.27 km² to 290.40 km² in 25 years (Figure 4 and Table 4). The expansion rate was measured to be 16.41 per cent, 16.47 per cent, 21.88 per cent, 16.36 per cent, 14.41 per cent and 13.53 percent respectively every four years in 1995, 1999, 2003, 2007, 2011 and 2015. Furthermore, the land cover of UMBA and the urban influencing outer peripheral area also increased due to changes in compactness

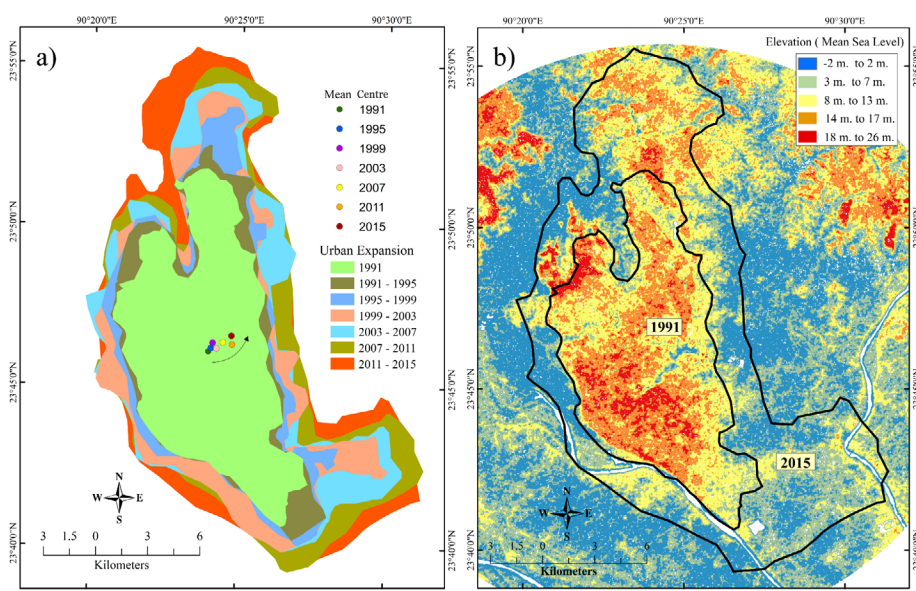


Figure 4. Map depicting: a) urban expansion with changing status of the absolute centre point, and b) Digital Elevation Model of the study area. The DEM was explored using 30 m spatial resolution SRTM data.

Table 4. Urban expansion and compactness ratio.

Year	Area	Expansion %	C_{oR}	Mean Centre Change (Direction)
1991	116.27	-	0.60	-
1995	135.35	16.41 %	0.63	0.25 Km North-Easterly
1999	157.64	16.47 %	0.57	0.32 Km North-North Easterly
2003	192.13	21.88 %	0.57	0.4 Km South-Easterly
2007	223.57	16.36 %	0.60	0.52 Km North-Easterly
2011	255.80	14.41 %	0.62	0.54 Km East-South-Easterly
2015	290.40	13.53 %	0.68	0.51 Km North

as evident in the urban compactness ratio (C_{oR}) measurements. The urban compactness ratio (C_{oR}) increased from 0.60 to 0.68 on a scale of 0 to 1. The mean centre of the urban area also changed due to a change in the compactness ratio (C_{oR}). The mean centre shifted from the actual mean centre in a north-easterly direction by a consequence of the urban compactness ratio (C_{oR}). The urban area has expanded to high elevated land and also to the low elevated land by land filling where wetland areas have been lost (Figure 4).

Table 3 presents the quantitative explanation of urban expansion, compactness ratio (C_{oR}), and shifting direction of the urban mean centre. The mean centre moved from the actual mean centre by 1.7 km in a north-easterly direction from 1991 to 2015. Urban expansion increased by 149.77 per cent from 1991 to 2015. The expansion rates were calculated to be 16.41 per cent, 16.47 per cent, 21.88 per cent, 16.36 per cent, 14.41 per cent and 13.53 per cent every four years, respectively in 1995, 1999, 2003, 2007, 2011 and 2015. Urban compactness areas saw an increase from 1999 to 2003, by 21.88 per cent.

Between 1991 and 2015, there was a significant acceleration in structural development and the expansion of built-up areas. This growth extended beyond the urban administrative boundaries into the surrounding rural areas, expanding urban boundaries beyond the metropolitan administrative areas. This expansion was mainly driven by a rapid increase in population density during that period (Streatfield & Karar, 2008; Ahmed & Bramley, 2015). In 2017, about 17 million people lived in Dhaka City. According to the Bangladesh Bureau of Statistics (BBS), the urban population increased at a rate of 113 percent from 1991 to 2011 (MOP-BD, 2013). The rapid population increase has directly influenced the demographic characteristics in urban expansion, changing urban compactness. The compactness ratio C_{oR} represents the shape of the urban area. The elevation profile of the study area was explored using DEM to find out which areas were most impacted by urban growth. The DEM showed that the urban area had extended from highlands to lowlands mainly because the wetland-dominated lowlands were more accessible and cheaper to develop.

UHI and physical footprints

UHI was detected to retrieve LST with seasonal variations. Table 5 represents the quantities of seasonal LST variations. In 1991 mean temperature was 21.86°C, 26.94°C and 23.16°C, respectively, during the winter, summer, and autumn seasons. 25 years later, in 2015, the mean temperature was measured at 24.26°C, 30.86°C, and 26.62°C, respectively, for the winter, summer, and autumn seasons. In the last 25 years,

Table 5. Seasonal minimum, mean and maximum land surface temperature (LST) ($^{\circ}\text{C}$) of the study area. Standard deviation and mean values included.

Year	Winter			Summer			Autumn		
	Minimum	Mean	Maximum	Minimum	Mean	Maximum	Minimum	Mean	Maximum
1991	15.2	21.86 ± 1.1	26.3	20.06	26.94 ± 1.04	33.59	17.09	23.16 ± 1.66	31.33
1995	12.14	20.95 ± 1.2	25.9	24.58	29.14 ± 0.72	34.54	17.18	23.39 ± 1.4	31.90
1999	13.33	24.98 ± 1.53	28.65	20.96	27.58 ± 1.38	36.83	17.75	23.43 ± 1.35	29.94
2003	13.21	25.96 ± 1.51	29.33	20.04	27.91 ± 1.74	35.76	16.63	23.88 ± 1.56	31.04
2007	14.6	24.09 ± 1.61	29.8	17.01	28.19 ± 1.39	38.77	19.9	23.67 ± 1.65	31.65
2011	14.42	24.48 ± 1.11	30.34	20.63	30.19 ± 1.48	39.28	18.93	24.94 ± 1.67	32.65
2015	10.9	24.26 ± 1.03	32.04	19.04	30.86 ± 1.79	42.22	18.34	26.62 ± 1.85	36.85

seasonal mean temperatures increased by 2.4°C , 3.92°C and 3.46°C , respectively, during the winter, summer, and autumn seasons.

An urban area's physical features (i.e. water bodies, vegetation, temperature, and structural bodies) are the main factors that contribute to changes in urban ecological footprints (Holden, 2004). Our research considers how physical footprints yield the characteristics of LULC change. The NDVI, NDWI, NDBI, and NDBaI indices represent the scenario of the physical footprints. Changes in LULC can influence the city's temperature variation. Table 6 demonstrates the relationship among LST, NDVI, NDWI, NDBI, and NDBaI indices. These four indicators are correlated with LST. While NDVI and NDWI values have a negative correlation with LST, the NDBI and NDBaI values have a positive correlation with LST. LST is the dependent value in this relationship, whereas NDVI, NDWI, NDBI, and NDBaI are independent values.

The LST is a dependent variable, and the other index values are independent values and negative and positive correlations were among these indicators. When temperature increases, NDVI and NDWI values decrease, representing a negative correlation. On the other hand, temperature increases with NDBI and NDBaI values, representing a positive correlation (Table 6). As land cover changes, physical footprints also change, resulting in an increase in LST.

Hot spot concentration of UHI

Hot spot analysis (G_i^*) delineated the geospatial pattern distribution of LST within a percentage of hot and cold confidence levels (Gi Bin). While a hot confidence level of more than 90 per cent was considered as a hot spot zone, a cold confidence level of more than 90 per cent was considered as a cold zone; finally, non-significant clusters were assumed to be stable zones. Figure 4 represents the spatial distribution of UHI using the nearest neighbour value with G_i^* consideration of UHI's changing status from 1991 to 2015. For example, from 1991 to 2015, cold spot areas increased from 19.40 km^2 to 50.36 km^2 . Within the same period, non-significant zones decreased from 236.90 km^2 to 162.14 km^2 while hot spot zones rapidly increased from 46.74 km^2 to 90.55 km^2 .

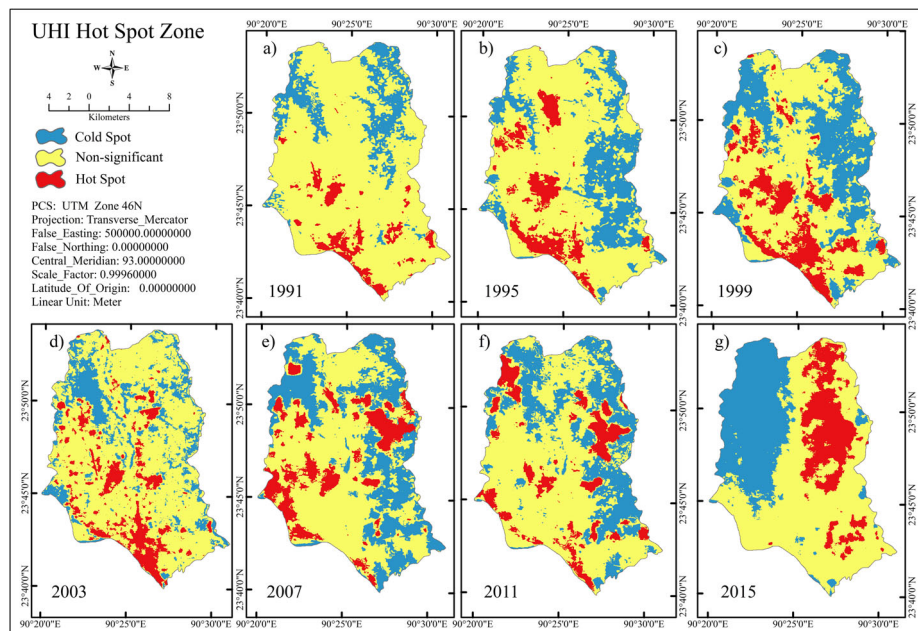
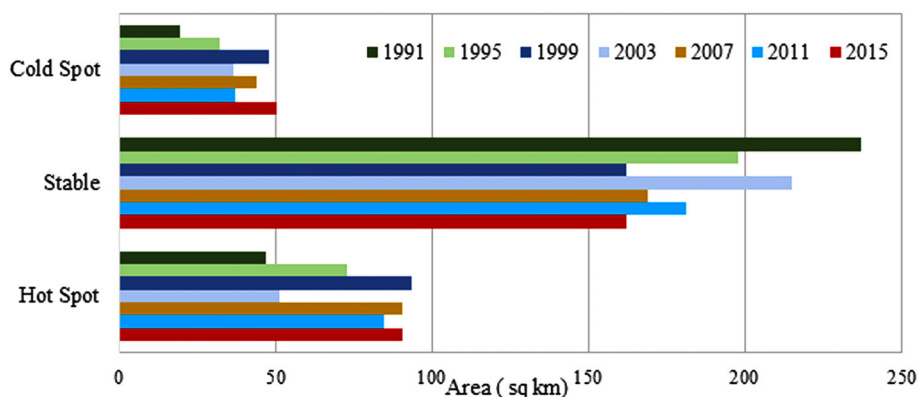
Figure 5 represents three geostatistical spatial categories of zones: i.e. (a) hot spot, (b) non-significant, and (c) cold spot. Each zone was demarcated based on data sourced within seven different periods from 1991 to 2015 in four-year intervals. During the last 25 years, cold spots increased by 10.21 percent; non-significant zones reduced by 24.67 percent; and hot spot areas increased by 14.46 percent (Figure 6). This demonstrates that temperature has increased, leading to the creation of hot zones. Conversely, although cold spots have also increased, the rate of increase is less than that of the hot spot areas. The decrease in non-significant areas represents the UHI's reduced stability, and temperature fluctuations.

Our hot spot analysis (G_i^*) generated the geospatial distribution of UHI in Dhaka megacity. This analysis produces a zone of categories that considers whole input pixels statistics and provides hot spot, non-significant, and cold spot categories within geographical coordinates. Hot spot analysis (G_i^*) is also advantageous because it produces each pixel's spatial distribution and geographic references with attribute data. Hot spot analysis (G_i^*) in the research was used to identify areas with higher temperatures compared to other regions within the study area. The analysis utilizes the nearest neighbour algorithm from geo-statistics to determine the spatial arrangement of these temperature hot spots. By applying this method, the research aims to allocate changing

Table 6. Correlation between LST and physical footprint indices.

	LST	NDVI	NDWI	NDBI	NDBaI
LST	1				
NDVI	-0.73	1			
NDWI	-0.77	0.71	1		
NDBI	0.88	-0.81	-0.92	1	
NDBaI	0.83	-0.78	-0.81	0.69	1

*The p-value is less than 0.05.

**Figure 5. Hot spot map of UHI (1991–2015).****Figure 6. Hot spot bar graph of UHI (1991–2015).**

temporal records to their corresponding spatial locations during a specific time interval. The information obtained from hot spot analysis helps understand the spatial patterns of temperature variations, which can inform decisions related to urban planning, environmental management, and climate adaptation strategies.

Seasonal SUHI intensity

SUHI intensity (Δ_T) was explored by calculating the difference between the mean LST of the UMBA and the mean LST of surrounding areas. The Δ_T was measured using 150 per cent of the controlling zone of UMBA area (i.e. 16.8 km distance between the mean urban centre and outer influencing boundary). We observed the intensity of UHI to be higher in the summer season as compared to autumn and winter (Table 7).

SUHI intensity increased by 2.95, 4.21, and 3.00, respectively in the winter, summer, and autumn seasons from 1991 to 2015 (Table 7). This reveals that UHI was not only affected in the UMBA but also in outer rural-urban marginal areas. The increasing trend of SUHI intensity impacts the local climate, ecosystem, and biodiversity of the UMBA as well as surrounding urban areas.

Discussion

Urban compactness in Dhaka has expanded by more than double in 25 years, urging the necessity for urban expansion to respond to the population's need for employment/jobs, and overall better quality of life. In addition, population density has increased due to migration into the city, which has led to urban expansion outside the metropolitan administrative zone. This unplanned urban growth was detected as the Urban compactness ratio (C_{oR}) which increased by 0.08 from 1991 to 2015, starting at 0.60 to 0.68 on the one scale. Although there was an increasing trend in C_{oR} that started from 16.41 percent in 1991 and continued until 2003 at 21.88 percent, this expansion rate cooled down to 13.53 per cent in 2015.

In the 25 years of study, water bodies have decreased by 19.48 per cent, vegetation cover has reduced by 24.23 per cent, while built-up areas and bare soil have experienced an increase of 33.84 per cent and 9.79 per cent, respectively—largely influenced by urban expansion and increasing population density. As temperature increased, NDVI and NDWI decreased, indicating a negative correlation. On the other hand, NDBI and NDBaI increased with rising temperature, indicating a positive correlation. With increased population density, built-up and bare soil areas have increased, resulting in increased movements, overuse of water and other resources, thereby negatively impacting vegetation growth due to less and less arable land area every year.

Table 7. SUHI intensity of study area.

Year	Δ_T (Winter)	Δ_T (Summer)	Δ_T (Autumn)
1991	1.20	0.87	1.10
1995	1.27	0.22	1.01
1999	1.34	3.14	1.14
2003	1.05	3.03	1.83
2007	1.30	3.97	1.58
2011	4.01	2.22	2.24
2015	4.15	5.08	4.10
$ \Delta_T$ 1991 to Δ_T 2015	2.95	4.21	3.00

In 1991, cold spot areas covered 19.40 km², however, by 2015, coverage had grown to 50.36 km². Between 1991 and 2015, non-significance zones decreased by 236.90 km² to 162.14 km², while hot spot zones increased by 46.74 km² to 90.55 km². In the winter, summer, and autumn seasons of the relevant period, SUHI intensity increased by 2.95, 4.21, and 3.00. As a result, UHI has impacted the UMBA and the surrounding rural-urban fringe areas.

Our research also detected seasonal variations in LST. LST levels were found to have increased during the winter, summer, and autumn seasons. In the last 25 years, seasonal mean temperature rose by 2.4°C, 3.92°C, and 3.46°C for the winter, summer, and autumn seasons. As population encroachment increases, green areas decrease, making it considerably challenging for the environment to cool down. This adds to the residual temperature effect every subsequent year, which—based on our findings—caused temperatures to rise within the relevant study period.

While urban green cover and water bodies have decreased over the last 25 years, built-up areas and bare soils have increased. Dhaka city has experienced 71.07 and 71.83 percent of water body and green coverage loss during the last 25 years, respectively. Simultaneously, built-up areas have increased by 147.74 percent. Due to a decrease in canals and wetlands, flooding was found to have occurred more frequently. We also observed a 3.26°C yearly average LST increase during the last 25 years. The methods and parameters used in detecting and analysing UHI in this study have constructed a clear image of change occurring over 25 years.

Conclusion

This study developed a method of deriving the future UHI of urban areas based on hot spot analysis as a means of finding out the status of land cover and temperature changes in Dhaka city during the period from 1991–2015. This study derived the UHI of Dhaka megacity based on hot spot analysis and represented significant and non-significant areas using long-term remote sensing data. Landsat 5 and 7 data were utilized to extract land cover, LST, UHI, and UMBA status. A series of data spanning 25 years was used to produce LST which was then translated into spatial and temporal UHI trends. Urban expansion and compactness were explored using the same dataset (i.e. Landsat 5 & 7 images). The urban compactness ratio (C_{OR}) represented the changing status of the mean centre. SRTM images were used to study the physical environment of the enlarged area. A series of Landsat 5 and 7 data spanning 25 years was also used to generate NDVI, NDWI, NDBI, and NDBaI to explore changes in the urban physical footprints arising from land cover change. NDVI, NDWI, NDBI, and NDBaI were used to examine the relationship between land cover change and LST trends. SUHI intensity (ΔT) is the status of UHI within influencing rural-urban fringe areas. As T_{Urban} and $T_{Boundary}$ were used to calculate SUHI intensity, SUHI intensity (ΔT) served as urban intensity indicators but also indicated the effect of UHI in surrounding rural areas. We employed LST for hot spot analysis (G_i^*) of UHI which demarcated UHI distribution into cooler areas, non-significant and hot spot zones. Our methodological framework may be applied to other cities and sites of urbanization.

Acknowledgements

We would like to thank the Community and Discussion for Environmental Research (CDER) research group for collecting field data for accuracy assessment and Professor Dr. Md. Mizanur

Rahman, Department of Geography and Environment, Jahangirnagar University, Dhaka, Bangladesh, for his valuable suggestions. We are sincerely grateful to the manuscript reviewers for their significant contributions and expertise, which greatly improved our work. We also extend our heartfelt appreciation to the journal editor panel for granting us the opportunity to publish our research.

References

- Ahmed B, Kamruzzaman M, Zhu X, Rahman M, Choi K (2013) Simulating land cover changes and their impacts on land surface temperature in Dhaka, Bangladesh. *Remote Sensing* **5** (11), 5969–98.
- Ahmed S, Bramley G (2015) How will Dhaka grow spatially in future? Modelling its urban growth with a near-future planning scenario perspective. *International Journal of Sustainable Built Environment* **4** (2), 359–77.
- Baddeley A, Berman M, Fisher NI *et al.* (2010) Spatial logistic regression and change-of-support in poisson point processes. *Electronic Journal of Statistics* **4**, 1151–1201.
- Bechtel B, Alexander P, Böhner J *et al.* (2015) Mapping local climate zones for a worldwide database of the form and function of cities. *ISPRS International Journal of Geo-Information* **4** (1), 199–219.
- Beverley H (1872) *Census of Bengal 1872*. The Bengal Secretariat Press, Calcutta.
- Cao L, Li P, Zhang L, Chen T (2002) Remote sensing image-based analysis of the relationship between urban heat island and vegetation fraction. *The International Archives of the Photogrammetry, Remote Sensing and Spatial Information Sciences* Vol. **XXXVI** (B7), 1379–84.
- Carlson TN, Traci Arthur S (2000) The impact of land use - land cover changes due to urbanization on surface microclimate and hydrology: a satellite perspective. *Global and Planetary Change* **25** (1–2), 49–65.
- Chakravorty S (1995) Identifying crime clusters: the spatial principals. *Middle States Geographer* **28**, 53–58.
- Chen F, Yang X, Zhu W (2014) WRF simulations of Urban Heat Island under hot-weather synoptic conditions: the case study of Hangzhou City, China. *Atmospheric Research* **138** (1), 364–77.
- Chen YH, Wang J, Li XB (2002) A study on urban thermal field in summer based on satellite remote sensing. *Remote Sensing for Natural Resources* **4**, 55–59.
- Chen XL, Zhao HM, Li PX, Yin ZY (2006a) Remote sensing image-based analysis of the relationship between Urban Heat Island and land use/cover changes. *Remote Sensing of Environment* **104** (2), 133–46.
- Chen M, Wang R, Zhang L, Xu C (2006b) Temporal and spatial assessment of natural resource use in China using ecological footprint method. *International Journal of Sustainable Development and World Ecology* **13** (4), 255–68.
- Chen Y (2011) Computers, environment and urban systems derivation of the functional relations between fractal dimension of and shape indices of urban form. *Computers, Environment and Urban Systems* **35** (6), 442–51.
- Damyanovic D, Reinwald F, Brandenburg C *et al.* (2016) Pilot Action City of Vienna – UHI-STRAT Vienna. In Musco F (ed) *Counteracting Urban Heat Island Effects in a Global Climate*, 257–81. Springer Nature, Cham.
- Decker EH, Elliott S, Smith FA, Blake DR, Rowland FS (2000) Energy and material flow through the urban ecosystem. *Annual Review of Ecology and Systematics* **26**, 685–740. Available at: <https://doi.org/10.1146/annurev.energy.25.1.685>.
- Deng C, Wu C (2012) BCI: a Biophysical Composition Index for remote sensing of urban environments. *Remote Sensing of Environment* **127**, 247–59.
- Deng Y, Srinivasan S (2016) Urban land use change and regional access: a case study in Beijing, China. *Habitat International* **51**, 103–13.
- Dos Santos AR, De Oliveira FS, Da Silva AG, Gleriani JM *et al.* (2017) Spatial and temporal distribution of Urban Heat Islands. *Science of the Total Environment* **605–606**, 946–56.

- Du H, Wang D, Wang Y et al. (2016) Influences of land cover types, meteorological conditions, anthropogenic heat and urban area on surface Urban Heat Island in the Yangtze River Delta urban agglomeration. *Science of the Total Environment* **571**, 461–70.
- Elmqvist T, Fragkias M, Goodness J et al. (eds) (2013) *Urbanization, Biodiversity and Ecosystem Services: Challenges and Opportunities*. Springer, Dordrecht.
- Fu P, Weng Q (2017) Responses of Urban Heat Island in Atlanta to different land-use scenarios. *Theoretical and Applied Climatology* **133**, 123–35.
- Gao B (1996) NDWI A Normalized Difference Water Index for remote sensing of vegetation liquid water from space. *Remote Sensing of Environment* **58** (April 1995), 257–66.
- Getis A, Ord JK (1992) The analysis of spatial association by use of distance statistics. *Geographical Analysis* **24** (3), 189–206.
- Gillies RR, Carlson TN (1995) Thermal remote sensing of surface soil water content with partial vegetation cover for incorporation into climate models. *Journal of Applied Meteorology* **34** (4), 745–56.
- Goh KC, Chang HC (1999) The relationship between height to width ratios and the heat island intensity at 22: 00 h. *International Journal of Climatology* **19** (9), 1011–23.
- Government of Bangladesh (GoB) (2010) The Bangladesh Environment Conservation (Amendment) Act, 2010. Available at: <https://bangladeshbiosafety.org/bangladesh-doc/bangladesh-environment-conservation-act-2010-amendment/>.
- Haggett P, Cliff AD, Frey A (1977) *Locational Analysis in Human Geography*, 2nd Edn. Edward Arnold Ltd, London.
- Holden E (2004) Ecological footprints and sustainable urban form. *Journal of Housing and the Built Environment* **19** (1), 91–109.
- Hossain S (2008) Rapid urban growth and poverty in Dhaka city. *Urban Studies* **5** (1), 1–24.
- Howard L (1833) The climate of London. *London Harvey Dorton* **2**, 1818–20.
- Hu L, Brunsell NA (2015) A new perspective to assess the Urban Heat Island through remotely sensed atmospheric profiles. *Remote Sensing of Environment* **158**, 393–406.
- Huang W, Li J, Guo Q et al. (2017) A satellite-derived climatological analysis of Urban Heat Island over Shanghai during 2000–2013. *Remote Sensing* **9** (7), 641. Available at: <https://doi.org/10.3390/rs9070641>.
- Hussain N, Islam MN (2020) Hot spot (Gi*) model for forest vulnerability assessment: a remote sensing-based geostatistical investigation of the Sundarbans mangrove forest, Bangladesh. *Modeling Earth Systems and Environment* **6** (4), 2141–51.
- Hussain N (2018) Water quality and status aquatic fauna of Dhaka Mega City, Bangladesh. *Sriwijaya Journal of Environment* **3** (2), 68–73.
- Jones PD, Groisman PY, Coughlan M, Plummer N, Wang W, Karl TR (1990) Assessment of urbanisation effects in time series of surface air temperature over land, 1990. *Nature* **347**, 169–72.
- Kabir A, Parolin B (2012) Planning and Development Of Dhaka – A Story Of 400 Years. Paper presented at the 15th International Planning History Society Conference, 15–18 Jul, Sao Paolo, 1–20.
- Kogan FN (1995) Droughts of the late 1980s in the United States as derived from NOAA polar-orbiting satellite data. *Bulletin - American Meteorological Society* **76** (5), 655–68.
- Kontoes CC (2008) Operational land cover change detection using change vector analysis. *International Journal of Remote Sensing* **29** (16), 4757–79.
- Li H, Zhou Y, Li X et al. (2018) A new method to quantify surface Urban Heat Island Intensity. *Science of the Total Environment* **624**, 262–72.
- Liu L, Zhang Y (2011) Urban Heat Island analysis using the Landsat TM data and ASTER data: a case study in Hong Kong. *Remote Sensing* **3** (7), 1535–52.
- Lu Y, Coops NC, Hermosilla T (2017) Estimating urban vegetation fraction across 25 cities in Pan-Pacific using Landsat time series data. *ISPRS Journal of Photogrammetry and Remote Sensing* **126**, 11–23.
- Mahdavi A, Kiesel K, Vuckovic M (2016) Counteracting Urban Heat Island effects in a global climate change scenario. In Musco F (ed) *Methodologies for UHI Analysis*, 71–91. Springer International Publishing, Cham.

- Maimaitiyiming M, Ghulam A, Tiyip *et al.* (2014) Effects of green space spatial pattern on land surface temperature: implications for sustainable urban planning and climate change adaptation. *ISPRS Journal of Photogrammetry and Remote Sensing* **89**, 59–66.
- McFeeters SK (1996) The use of the Normalized Difference Water Index (NDWI) in the delineation of open water features. *International Journal of Remote Sensing* **17** (7), 1425–32.
- Meng Q, Zhang L, Sun Z, Meng F, Wang L, Sun Yunxiao (2018) Characterizing spatial and temporal trends of surface Urban Heat Island effect in an urban main built-up area: a 12-year case study in Beijing, China. *Remote Sensing of Environment* **204** (November 2016), 826–37.
- Miles V, Esau I (2017) Seasonal and spatial characteristics of Urban Heat Islands (UHIs) in northern west Siberian cities. *Remote Sensing* **9** (10), 989. Available at: <https://doi.org/10.3390/rs9100989>.
- Karim MF, Haider MJ (2003) Engineering geology and geomorphology for ground improvement in the Dhaka City - Tongi Area. *Atlas of Urban Geology* **14**, 187–94.
- MOP-BD (2013) *District Statistics, Ministry of Planning*. Government of Bangladesh, Dhaka.
- Newman PWG (1999) Sustainability and cities: extending the metabolism model. *Landscape and Urban Planning* **44** (4), 219–26.
- Nichol J, Wong MS (2005) Modeling urban environmental quality in a tropical city. *Landscape and Urban Planning* **73** (April 2004), 49–58.
- Oke TR, Cleugh HA (1987) Urban heat storage derived as energy balance residuals. *Boundary-Layer Meteorology* **39** (3), 233–45.
- Ord JK, Getis A (1995) Local spatial autocorrelation statistics: distributional issues and an application. *Geographical Analysis* **27** (4), 286–306.
- Orhan O, Ekercin S, Celik F (2014) Use of Landsat land surface temperature and vegetation indices for monitoring drought in the Salt Lake Basin Area, Turkey. *The Scientific World Journal* 2014 (Vci). Available at: <https://doi.org/10.1155/2014/142939>.
- Peng S, Piao S, Ciais P *et al.* (2012) Surface Urban Heat Island across 419 global big cities. *Remote Sensing of Environment* **46** (12), 3175–86.
- Qian LX, Cui HS, Chang J (2006) Impacts of land use and cover change on land surface temperature in the Zhujiang Delta. *Pedosphere* **16** (200523), 681–89.
- Rabeya R (2017) Re-Defining Courtyard to Re-Vitalize Urban Community. In Proceedings of UIA 2017 Seoul World Architects Congress; 3–10 Sept 2017, Seoul, Korea. UIA, Seoul.
- Rahman HZ (2014) Urbanization in Bangladesh: challenges and priorities. Paper presented at Bangladesh Economists' Forum, Jun 21–22, Dhaka, Bangladesh.
- Rayk R, Kapp R, Reuter U *et al.* (2016) Pilot actions in European cities – Stuttgart. In Musco F (ed) *Counteracting Urban Heat Island Effects in a Global Climate Change Scenario*, 281–305. Springer International Publishing, Cham.
- Rodriguez Lopez JM, Heider K, Scheffran J (2017) Frontiers of urbanization: identifying and explaining urbanization hot spots in the south of Mexico City using human and remote sensing. *Applied Geography* **79**, 1–10.
- Roth M, Chow WT (2012) A historical review and assessment of urban heat island research in Singapore. *Singapore Journal of Tropical Geography* **33** (3), 381–97.
- Rosenzweig C, Karoly D, Vicarelli M *et al.* (2008) Attributing physical and biological impacts to anthropogenic climate change. *Nature* **453** (7193), 353–57.
- Scott L, Warmerdam N (2005) Extend crime analysis with ArcGIS spatial statistics tools. *ArcUser Online* April-June **8** (2). Available at: https://www.esri.com/news/arcuser/0405/ss_crimestats2of2.html.
- Shahfahad NMW, Towfiqul Islam ARM, Mallick J, Rahman A (2022a) Land use/land cover change and its impact on surface urban heat island and urban thermal comfort in a metropolitan city. *Urban Climate* **41**, 101052. Available at: <https://doi.org/10.1016/j.uclim.2021.101052>.
- Shahfahad, Talukdar S, Rihan M, Hang HT, Bhaskaran S, Rahman A (2022b) Modelling urban heat island (UHI) and thermal field variation and their relationship with land use indices over Delhi and Mumbai metro cities. *Environment, Development and Sustainability* **24** (3), 3762–90.

- Sobstyl JM, Emig, T. Qomi, MA, Ulm FJ, Pellenq RM (2018) Role of city texture in urban heat islands at nighttime. *Physical Review Letters* **120** (10), 108701. Available at: <https://doi.org/10.1103/PhysRevLett.120.108701>.
- Souch C, Grimmond S (2006) Applied climatology: urban climate. *Progress in Physical Geography* **30** (2), 270–79.
- Streatfield PK, Karar ZA (2008) Population challenges for Bangladesh in the coming decades. *Journal of Health, Population and Nutrition* **26** (3), 261–72.
- Streutker DR (2002) A remote sensing study of the Urban Heat Island of Houston, Texas. *International Journal of Remote Sensing* **23** (13), 2595–608.
- Taleb MA (2012) Comparative study of urban area extension and flood risk in Dhaka City of Bangladesh. *Global Journal of Human Social Science Geography & Environmental Geosciences* **12** (11), 37–40.
- Tan J, Zheng Y, Tang X et al. (2010) The urban heat island and its impact on heat waves and human health in Shanghai. *International Journal of Biometeorology* **54**, 75–84.
- The Daily Star* (2012) High Court ruling on illegal landfill welcome. Editorial, 1 August. Available at: <https://www.thedailystar.net/news-detail-244281>.
- The Daily Star* (2019) Stop earth-filling by 24 companies. Staff Correspondent, 28 January. Available at: <https://www.thedailystar.net/country/ensure-status-quo-earth-filling-in-purbachal-high-court-1693570>.
- Tran DX, Pla F, Latorre-Carmona P, Myint SW, Caetano M, Kieu HV (2017) Characterizing the relationship between land use land cover change and land surface temperature. *ISPRS Journal of Photogrammetry and Remote Sensing* **124**, 119–32.
- United Nations Economic and Social Commission for Asia and the Pacific (UNESCAP) (2003) Review of Developments in Transport in the ESCAP Region 2003. United Nations, New York.
- United Nations Human Settlement Programme (UN-Habitat) (2020) Unpacking the value of sustainable urbanization. In *World Cities Report 2020*. UN-Habitat, Nairobi.
- USGS (2011) *Landsat 7 Science Data Users Handbook*. The United States Geological Survey, Reston. Available at: <https://www.usgs.gov/landsat-missions/landsat-7-data-users-handbook>
- Vinayak B, Lee HS, Gedam S, Latha R (2022) Impacts of future urbanization on urban microclimate and thermal comfort over the Mumbai metropolitan region, India. *Sustainable Cities and Society* **79**, 103703. Available at: <https://doi.org/10.1016/j.scs.2022.103703>.
- Wackernagel M, Schulz NB, Deumling D et al. (2002) Tracking the ecological overshoot of the human economy. In *Proceedings of the National Academy of Sciences* **99**, 9266–71.
- Walawender JP, Szymanowski M, Hajto MJ, Bokwa A (2014) Land surface temperature patterns in the urban agglomeration of Krakow (Poland) derived from Landsat-7/ETM+ data. *Pure and Applied Geophysics* **171** (6), 913–40.
- Wolman A (1965) The Metabolism of Cities. *Scientific American* **213** (3), 156–74.
- Yao R, Wang L, Huang X, Niu Z, Liu F, Wang Q (2017) Temporal trends of surface Urban Heat Islands and associated determinants in major Chinese cities. *Science of the Total Environment*, **609**, 742–54.
- Zha Y, Gao J, Ni S (2003) Use of normalized difference built-up index in automatically mapping urban areas from TM imagery. *International Journal of Remote Sensing* **24** (3), 583–94.
- Zhang J, Wang Y (2008) Study of the relationships between the spatial extent of surface Urban Heat Islands and urban characteristic factors based on Landsat ETM + Data. *Sensors* **8** (11), 7453–68.
- Zhao H, Chen X (2005) Use of normalized difference bareness index in quickly mapping bare areas from TM / ETM +. In *Proceedings of the 2005 IEEE International Geoscience and Remote Sensing Symposium; 29 Jul, Seoul, Korea*. IEEE, Piscataway.